Infection, Genetics and Evolution 81 (2020) 104210

Contents lists available at ScienceDirect

Infection, Genetics and Evolution

journal homepage: www.elsevier.com/locate/meegid

Research paper

Acarbose, as a potential drug, effectively blocked the dynamic metastasis of EV71 from the intestine to the whole body

Qingyuan Feng[b,1], Huiting Zhou[a,1], Xiyue Zhang[c,1], Xuan Liu[a], Jie Wang[a,1], Cuiping Zhang[a,1], Xiaojing Ma[a], Chunju Quan[a], Zhongliang Zheng[a,*]

[a] State Key Laboratory of Virology, College of Life Sciences, Wuhan University, Wuhan 430072, China
[b] Department of Otorhinolaryngology Head and Neck Surgery, The First Affiliated Hospital of Guangxi Medical University, Nanning, Guangxi 530021, China
[c] China Animal Health and Epidemiology Center, Qingdao, Shandong 266032, China

ARTICLE INFO

Keywords:
EV71
Dynamic pathway
Intestine
Intestinal absorption inhibitor
Acarbose
Physiological mechanism

ABSTRACT

Enterovirus 71 (EV71) is one of the main pathogens causing hand-foot-and-mouth disease (HFMD). The nose and mouth are usually the main infection entries of EV71 virus. However, its dynamic transport pathway from mouth to the whole body remains unknown. The reveal of this physiological mechanism *in vivo* will help to understand its transport direction, find its key proliferation nodes, and develop new preventive strategies. We trained a new strain of GFP-EV71 virus to be susceptible to mice brain by intracranial injection of mice. The adapted virus was oral-administrated to suckling mice. Then, the dynamic distributions of the virus *in vivo* were detected by living image system and fluorescence quantitation polymerase chain reaction (qPCR). We figured out the dynamic pathway of EV71 transport *in vivo* from intestine to peripheral tissue, then to the other organs. Small intestine was identified as a gateway for EV71 infection *in vivo*. Ileum was proved to be the main part of proliferation and transport of EV71 in small intestine of mice. EV71 was verified to enter small intestinal villus of mice through the infection of small intestinal epithelial cell. Acarbose displayed a good preventive effect on EV71 infection both *in vivo* and *in vitro*. Acarbose possibly decreased the intestinal infection of EV71 by blocking the receptor-binding sites on the surface of EV71 virion or by inhibiting various glycolic receptors on the cell surface. Thus, acarbose and its analogue may be the potential medicines to prevent EV71 infection.

1. Introduction

HFMD is an easily contagious viral infection which affects infants and children under five years of age. Recently, severe outbreaks of HFMD were reported frequently in the Asia-Pacific region, including China and Korea (Yi et al., 2017). The main cause of HFMD is coxsackievirus A16 (CVA16) or enterovirus 71 (EV71) infection (He et al., 2013). Although CVA16 triggers more incidence of HFMD, EV71 as a neurotropic virus frequently bring about more severe consequences including pulmonary edema, neurological symptoms and heart disease, even death (Solomon et al., 2010; Zhou et al., 2011). Therefore, it is urgent to find an effective treatment against EV71.

Previous studies on EV71 have noted the importance of several subjects, such as novel antiviral drugs (Chang et al., 2013; Hung et al., 2014; Kim et al., 2016; Xu et al., 2016; Zhang et al., 2013), functional mechanisms of diversified structural proteins (Caine et al., 2016; Cong et al., 2016; Lei et al., 2017; Li et al., 2017; Victorio et al., 2016), clinical features (Zeng et al., 2016), infectious pathways (Lee, 2016) and infected animal models (Lin et al., 2013), while few report was found on prevention of EV71 infection because of the unknown physiological transport mechanism in human body.

Clinical features indicate that EV71 infection primarily leads to papulovesivular rash on the palms and soles, and multiple oral ulcers. Other syndromes include gastroenteritis, pneumonia, aseptic meningitis, and brainstem encephalitis (24). Although it is sure that the oral cavity is the main port of entry for EV71 infection, the dynamic physiological pathway of EV71 transporting from oral cavity to the whole body is still unknown, due to the complication of human internal environment (Song et al., 2018; Yao et al., 2018). So the exploration of this mechanism is of great significance, meanwhile the prevention of intestinal infections will promote the development of new treatments.

Lintao Cai et al. (Pan et al., 2018) found that the different

Abbreviations: CPE, cytopathic effect; MOI, multiplicity of infection; SCARB2, Scavenger Receptor Class B Member 2

* Corresponding author.
E-mail address: biochem@whu.edu.cn (Z. Zheng).

[1] Contributed equally to this work.

https://doi.org/10.1016/j.meegid.2020.104210
Received 7 November 2019; Received in revised form 31 December 2019; Accepted 27 January 2020
Available online 28 January 2020
1567-1348/ © 2020 Elsevier B.V. All rights reserved.

pathogenicity of EV71 displayed various transmission routes and tissue tropisms. His group utilized orthogonal fluorescence labeling *in situ* and revealed the difference of viral dynamics, dissemination and tissue tropism between severe case EV71 (SC-EV71) and mild case EV71 (MC-EV71). SC-EV71 was found to have stronger ability of invading blood circulation and spreading out. SC-EV71 also displayed neuronal and respiratory tropism.

In this study, we adopted creative strategies to illustrate the dynamic transport pathway of EV71 infection *in vivo*. GFP-EV71 was firstly adapted as the virus susceptible to mice nerve infection. Then, the dynamic transport pathway of EV71 was affirmed in mice through dissecting oral-administrated suckling mice. We sequentially conducted in-depth study on the physiological mechanism of EV71's intestine infection in order to explore the possibility of infection prevention. SCARB2 is the cellular receptor of EV71 infection. EV71 infection relies on the interaction of the canyon region of its virion surface and the glycosylation of SCARB2 protein (Dang et al., 2014; Li et al., 2013). Thus, the right glycosyl group will competitively inhibit EV71 infection. The suppression of intestinal infections will effectively prevent EV71 from invading the whole body. We chose acarbose as the inhibitor of EV71 infection, based on its more pyran glucose groups. Acarbose is also an intestinal absorption inhibitor which can efficiently block glucose absorption through its pyran glucose groups in intestine. So acarbose possesses the potential not only to inhibit cellular receptors of various glycosylated viruses but also to competitively block the canyon region of EV71 virion surface (Dang et al., 2014).

2. Materials and methods

2.1. Mice

One-day-old ICR (Institute of Cancer Research, ICR) suckling mice were used in the experiment. The suckling mice were obtained from the Hubei Provincial Center in China for Disease Control and Prevention. Each cage has a minimum of seven mice. All animal experiments were performed according to animal care and welfare protocols. Prior approval has been obtained from the Institutional Review Board (IRB) of China.

2.2. Cell lines and cell culture

Human rhabdomyosarcoma (RD) cells (ATCC No.CCL-136), human colon fibroblast cells (CCD18-Co) cells (ATCC No.CRL-1459), human colorectal adenocarcinoma epithelial (DLD-1) cells (ATCC No.CCL-221), human colon epithelial (FHC) cells (ATCC No.CRL-1831) and mouse neuroblastoma neuroblast (Neuro-2a) cells (ATCC No.CCL-131) were provided by China Center For Type Culture Collection (CCTCC). RD cells, CCD18-Co cells and FHC cells were cultured in Dulbecco's modified Eagle's medium (DMEM) containing 10% fetal bovine serum (FBS) (Tianhang Ltd., China). DLD-1 cell line was maintained in RPMI-1640 Medium containing 10% FBS. Neuro-2a cell line was maintained in Eagle's Minimum Essential Medium (EMEM) containing 10% FBS. All cells were cultured in a humidified atmosphere containing 5% CO_2 at 37 ˚C. All culture reagents were purchased from Life Technologies Ltd. …

2.3. Virus culture and titration assay

EV71 SK-EV006 wild strain, as one of MC-EV71, was obtained from Dr. Satoshi Koike (Kobayashi et al., 2018). Virus multiplication was performed in RD cells. Pure virus was diluted into 2 ml DMEM medium containing no FBS. Took a 10 cm petri dish containing about 70% confluence of RD cells and removed the original medium. Tiled the medium containing EV71 virus into the petri dish. After 4 h of infection, supplied 10 ml EMEM medium containing 10% FBS. Then incubated for 36 h. Scraped the cells and suspended the cells in 1 ml phosphate buffer solution (PBS). Lysed the cells by freezing in liquid nitrogen and thawing at 37 ˚C. Centrifuged the cells and collected the supernatant. Divide the supernatant into three parts and respectively inoculate them into the new petri dishes containing 70% confluence of RD cells. Repeated above processes for two times. Then 27 dishes of infected cells were obtained for further virus purification.

Virus purification was based on using a cesium chloride (CsCl) density gradient combined with ultracentrifugation. From top to bottom of centrifuge tube, the liquid layers should be as follows: 1 ml cell lysate, 3 ml 1.2 g/ml CsCl and 3 ml 1.4 g/ml CsCl. After centrifuging for 4 h at 35,000 rpm, we observed a white band locating at the center of the tube, where CsCl should have a density of 1.3 g/ml. We used a needle and syringe to take out the white virus-containing band from the centrifuge tube. Then, performed dialysis in PBS buffer and stored at −80 ˚C. To titrate the purified GFP-EV71, the 100 μl virus stocks were serially diluted from 10^{-1} to 10^{-10} fold in DMEM medium and incubated with the RD cells. Cells were grown in 96-well cell culture microtiter plates for 12 h at 37 ˚C. DMEM medium with no virus was added to RD cells as negative control. Viral titers were determined by a cytopathic effect (CPE) assay under inverted microscope each day. After 3 days, the endpoint titer was calculated in tissue culture infective dose 50 ($TCID_{50} = 10^{6.33}$/ml) as described by Reed and Muench (Zhao et al., 2017). When RD cells were infected with the purified virus at multiplicity of infection (MOI) of 3.0, 95% of RD cells displayed CPE in 24-well cell culture plate after 2 days.

2.4. Virus adaptation

All mice were reared under specific-pathogen-free conditions in individually ventilated cages. 1-day-old ICR neonatal suckling mice were inoculated with purified GFP-EV71 *via* intracranial injection. 3 days later, we qualitatively observed the proliferation stage of virus particles in murine brains with LuminaIILiving Image System (Caliper LifeSciences Ltd., Model. IVIS Lumina II). Other tissues displaying large amount of GFP fluorescence were collected and homogenized in physiological saline. Total RNA was extracted from different tissues such as brain, muscle, lung, intestine, and so on. RNA levels of EV71 were measured by reverse transcription-polymerase chain reaction (RT-PCR). Meanwhile, homogenization buffer containing viruses were inoculated into RD cells. New generation of GFP-EV71 were amplified and purified after 7 days of cell culture time. Repeated the above processes until all injected mice displayed bright GFP fluorescence in brain tissues. Finally, we obtained mouse-adapted EV71 virus strain. The capsid protein genes including VP1, VP2 and VP3 were sequenced by primers that Dr. Satoshi Koike has used (Yamayoshi et al., 2009). The first pair of primers were GFP-AITTL-VP4-F (5′- CTTGGCTCACAAGTGTCTACT −3′) and SK-EV-1908-R (5′- AAACTGGTAGCATTGGTGGGT −3′). The second pair of primers were SK-EV-1888-F (5′- ACCCACCAATGCTACC AGTTT −3′) and SK-EV-2982-F (5′- ACAAAAACTGAGGGGTTTGT −3′). The last pair of primers were SK-EV-2783-F (5′- GGTTACGCAC AGATGCGCAG −3′) and SK-EV-3340-R (5′- GAACTTTCCAAGGGTAG TAATG −3′).

2.5. Oral administration of suckling mice

36 newborn 1-day-old ICR murine were divided randomly into two groups. The mice of experimental group were orally treated with 10 μl GFP-EV71 (MOI = 3). The mice of control group were mock-infected with 10 μl normal saline. Then, both of groups were suckled by their mother mice. Every 24 h, the dynamic distribution of green florescence was detected in LuminaII Living Image System. At the same time, we dissected three suckling mouse respectively from the experimental group and the control group to get tissue samples including brain, heart, blood, intestine, kidney, liver, lung, muscle, spleen and stomach. Changes of EV71 virus titer in those tissues were then detected by qPCR.

2.6. Histology assay

Intestine tissues were harvested from euthanized mice and immediately fixed with 10% formalin for 48 h at room temperature. Then rinsed, dehydrated the tissues. The fixed tissues were paraffin embedded, sectioned, and stained with hematoxylin and eosin (H&E) or a rabbit anti-EV71 VP1 monoclonal antibody (GeneTex Ltd. Cat No. GTX132339) (Khong et al., 2012). The GFP fluorescence of sections were directly observed under a fluorescence microscope.

2.7. Immunohistochemistry (IHC) assay

Paraffin embedded tissue sections were re-hydrated through xylene (3 times at 5 min each) and a series of graded alcohols (EtOH) (100% EtOH for 2 times, 95% EtOH for 1 time, 70% EtOH for 1 time. Distilled water for 2 times. Each time at 5 min). Sections were treated with 0.01% Triton-X100 and subjected to antigen retrieval using sodium citrate solution in a pressure cooker for 5 min and allowed to cool (Lin et al., 2015). Then the slides were washed, blocked, and labeled with rabbit anti-EV71 VP1 antibody (GeneTex Ltd. Cat No. GTX132339) according to the manufacturer's procedures of Rabbit Primary Histostain-Plus IHC Kit (Neobioscience Ltd. Cat No. ENS004.300). Control sections for each antibody were stained without primary antibody. Two hours later, washed the slides and incubated with horse radish peroxidase (HRP)-linked goat anti-rabbit antibody (Amyjet Scientific Ltd. Cat No. 6401–05). Then, add 3,3′-diaminobenzidine (DAB) to launch brown reaction. HRP will catalyze DAB into a dark brown reaction product and result in a brown, alcohol-insoluble precipitate at the site of target antigens.

2.8. The intestinal absorption assay of mice model

Acarbose (Selleck Ltd. Cat No. S127101) was chosen as the intestinal absorption inhibitor, while sodium caprate was used as the intestinal absorption enhancer. Acarbose is also an intestinal absorption inhibitor which can efficiently block glucose absorption through its pyran glucose groups in intestine. So acarbose possesses the potential not only to inhibit cellular receptors of various glycosylated viruses but also to competitively block the canyon region of EV71 virion surface (22). Therefore, 72 newborn 1-day-old ICR murine were divided randomly into 4 groups - enhancer group, inhibitor group, negative control group and positive control group. Firstly, the enhancer group was oral-administrated with 10 μl of sodium caprate (0.45 μg/μl) , and the inhibitor group was treated by 10 μl of acarbose (0.45 μg/μl). At the same time, the other two groups were orally injected with 10 μl of normal saline. After 10 min, three groups of mice except negative control group, were orally injected with 10 μl mixture of GFP-EV71 (MOI = 3) and pure milk in the ratio of 1:1. Then the enhancer and inhibitor groups were orally injected with 10 μl of drug every 12 h. Meanwhile, we dissected three suckling mouse from each group every 12 h, and took intestine samples. After 72 h, all samples were used for qPCR analysis.

2.9. qPCR

The expression of VP1 (the critical capsid protein of EV71) was assayed by qPCR. Total RNA was extracted from tissues or cells by using Trizol (Life Technologies Ltd.) according to the manufacturer's instructions. Reverse transcription was performed with 3 μg of total RNA, oligo(dT) and RevertAid Reverse Transcriptase (Thermo Fisher Scientific) according to the supplier's instructions. qPCR was performed with SuperReal PreMix SYBR Green (TIANGEN) in the Applied Biosystems 7500 Fast Real-Time PCR System (Life Technologies Ltd.). $2^{-\triangle\triangle Ct}$ method was used to calculate the fold change of VP1 RNA level between different cells. The expression levels were normalized using human GAPDH (glyceraldehyde-3-phos-phate dehydrogenase). PCR primers included (5'to 3′) VP1 sense (ACGCGCAAATGCGTAGAAA GGT), VP1 antisense (TTAGTGGCAGTTTGCCATGCGA).

2.10. Knock-down assay through siSCARB2

The small interfering RNA (siRNA) was used for the knockdown of SCARB2 in cells. The following siRNA sequences target the human SCARB2 coding region, GUAUCGAGAAGAAAAUUGU (Guangzhou RiboBio Ltd.). A scramble siRNA (UUC UCC GAA CGU GUC ACG UTT) (Guangzhou RiboBio Ltd.) was used according to the manufacturer's recommendations. Cells were cultured in a 60-mm culture vessel until cell confluence reached 80%, and then transfected 50 nmol of siSCARB2 by using Lipofectamine 2000 (ThermoFisher Ltc. Cat No. 11668019). After 48 h' incubation, cells were subsequently infected with EV71 (MOI = 3), and treated with acarbose (1.5 μg/ml) or sodium caprate (1.5 μg/ml) during the next 24 h.

2.11. Western blot assay

5 μg of protein were separated on 10% SDS-PAGE gels and transported to polyvinylidene difluoride membranes. Specific primary antibodies were incubated separately with the membranes at 4 °C overnight after blocking with 5% nonfat milk, and the membranes were then probed with corresponding peroxidase-labeled secondary antibodies for 1.5 h at room temperature. SuperSignal West Dura Extended Duration Substrate (Pierce Chemical) was used to detect horseradish peroxidase (HRP) according to manufacturer's instructions. Antibodies mentioned above included rabbit anti-EV71-VP1 antibody (GeneTex Ltd. Cat No. GTX132339), rabbit anti-SCARB2 antibody (Proteintech Ltd., Cat NO. 27102–1-AP), mouse anti-GAPDH antibody (Proteintech Ltd., Cat NO. 60004–1-Ig), HRP-linked goat anti-rabbit antibody (Amyjet Scientific Ltd. Cat No. 6401–05), and HRP-linked goat anti-mouse antibody (Proteintech Ltd., Cat NO. SA00001–1).

2.12. Flow cytometry assay

RD cells, DLD-1 cells, FHC cells and CCD18-Co cells were collected for concentration adjustment to 1×10^6/ml after 36 h of GFP-EV71 infection. Total cell suspensions were prepared as described previously (Khong et al., 2012). Data were acquired using Cyan flow cytometer with the Summit software (Beckman Coulter).

3. Results

3.1. Adaption training of GFP-EV71 in suckling mice

Original GFP-EV71 was obtained from Dr. Satoshi Koike. Its prototype was EV71 SK-EV006 wild strain (Yamayoshi et al., 2009). Though EV71 SK-EV006 wild strain prefers muscular tissues, we expected that it could also infect nervous tissues through adaption, so that we could explore the intact transport pathway from intestine to muscle, then to brain. On account of the immune clearance of adult mice, we chose suckling mice to conduct the experiments, in which purified viruses were injected into the brains of suckling mice for EV71 adaption.

Purified GFP-EV71 was inoculated intracranially into suckling mice for three times until GFP-EV71 was adapted to the mice brain. Though GFP fluorescence faded away as the number of injections increases, we reconstructed newly generated brain-adapted virus into a new generation of GFP-EV71 according to Dr. Satoshi Koike's method (Yamayoshi et al., 2009). The injected mice primitively displayed severe behavior chaos including shiver, drooling, fever, spasm, even quick death. After three times of reconstruction, a new GFP-EV71 was successfully adapted to mice brain tropism though less virulent. The main behavior chaos reduced to some extent, such as reduced number of spasms and decreased mortality. As shown in Fig. 1A, after 3 days, the adapted GFP-EV71 displayed bright green fluorescence (green arrow), while red

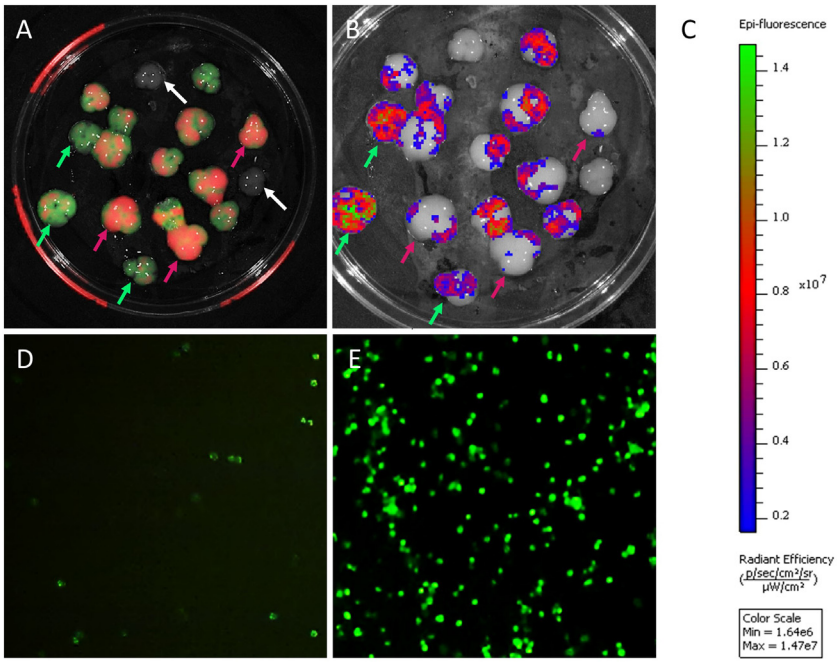

Fig. 1. Detection of the adaptability of GPF-EV71 by viral brain injection and nerve cell infection. (A) Detection of GFP fluorescence in suckling mice brains by Lumina IILiving Image System. 20 µl of GFP-EV71 (MOI = 3) were applied for mice cerebral injection. (B) Color-scale measurement of fluorescence intensity in suckling mice brains by Lumina IILiving Image System. (C) Color scale of Epi-fluorescence in Lumina IILiving Image System. (D) Detection of GFP fluorescence in Neuro-2a cells by microscope. Neuro-2a cells were infected by original unadapted GFP-EV71 (MOI = 3). (E) Detection of GFP fluorescence of Neuro-2a cells by microscope. Neuro-2a cells were infected by adapted GFP-EV71 (MOI = 3).

fluorescence (red arrow) was perhaps produced by degrading virus particles. There was no fluorescence in non-injection brains (white arrow). Fluorescence intensities were quantified through calculating color scale by LuminaIILiving Image System as shown in Fig. 1B and C. After sequencing the VP1/VP2/VP3 region of new GFP-EV71, we found several significant mutants including two VP1 sites (Gly88 → Ser88, Lys244 → Asp244), two VP2 sites (Phe158 → Ser158, Ala228 → Ser228) and one VP3 site (Pro59 → Ser59). According to the capsid protein structure of EV71 (Lyu et al., 2015), these mutant sites encode the modifiable residues which located on the surface of virus particle. Therefore, we speculated that the virus changed the glycosylation of its capsid proteins when adapting to mice brain. New glycosylation might help EV71 to bind a certain cell surface receptor of saccharide groups.

Subsequently, the brain-harvested GFP-EV71 was used to infect Neuro-2a (mouse neuroblast) cells in order to verify its neurotropic character. As shown in Fig. 1D and E, the Neuro-2a cells were infected efficiently by the adapted GFP-EV71 and displayed more fluorescences than those infected by original GFP-EV71 strain. This adapted GFP-EV71 strain was further used in oral-administration.

3.2. Dynamic process of EV71 proliferation and transportation from small intestine

The nose and mouth are the main entry points for infection for EV71 virus entering human body. Similar to Che-Szu Chen's method (Chen et al., 2007), we tried to simulate the real process of EV71 infection in mice through oral-administration. 1-day-old suckling mice were oral-administrated by GFP-EV71, and the dynamic distribution of GFP-EV71 was detected by Lumina & Living Image System every 24 h. As shown in Fig. 2A, in the first day after oral-administration, there was a lot of green fluorescence accumulating in the mice abdomen. Green Fluorescence resulted from the oral infusion of virus. These viruses had not been totally excreted or transferred in time. The decay of green fluorescence in the second day indicated a huge decrease of virus in abdomen, which means most viruses were excreted out of bodies while some transferred into other body parts. The feces excreted on the first and second day were checked and showed very weak green fluorescence. At the third day, Green fluorescence presented in peripheral tissues including limbs, tails and ears, which meant that GFP-EV71 had spread into blood through infected intestine cells and proliferate in peripheral tissues again. In the fourth and fifth days, green fluorescence decayed relatively, but was still visible in backs and peripheral tissues.

Although the spread of virus could not be traced by GFP, which only presented during EV71-mRNA translation in host cells, VP1 staining and real-time PCR can expediently indicate tracks of EV71 virus. VP1 protein is the capsid protein of EV71. VP1 protein has usually been considered as an indicator of eliciting a protective immune response after EV71 infection.(Fan Gao et al., 2012) Therefore, we extracted total RNA from different mice tissues to quantify virus proliferation. The VP1 mRNA representing mRNA levels of EV71 was detected every 24 h after oral-administration, and the results displayed a clear tendency of virus transport and proliferation in mice bodies as shown in Fig. 2B. The result also showed a consistently low level of EV71 in blood. These evidence indicated that EV71 entered the blood circulation and spread quickly (Pan et al., 2018). So we used blood as the negative control. Heart tissues displayed the same tendency as blood. Interestingly, EV71 mRNA levels in mice intestinal tissues showed more than a 10-fold increase at the second day, but reduced by half at the third day, then returned to nearly 12 fold at the fourth day, finally exceeded more than 20-folds at the fifth day. This showed that EV71 had experienced a process of proliferation, transport and proliferation outbreak in mice intestines. Mice muscle tissues were taken from mice hind legs. Large numbers of blood capillaries existing in legs, facilitated EV71 to park and spread. According to the qPCR result, EV71 mRNA levels in the muscle tissue rose suddenly and sharply at the third day and kept increasing at the following two days, which indicated muscle tissues were the second place to be invaded by EV71. The fourth and fifth days were the whole-body-outbreak period, for EV71 mRNA levels remained relatively higher in other organs, such as brain, kidney, liver, lung, spleen and stomach.

Obviously, EV71 firstly proliferated in mice intestinal tissues at the second day after oral-administration. Then EV71 transported quickly through blood and multiplied in peripheral tissues at the third day. The fourth and fifth days were the outbreak period in the whole bodies of mice. EV71 already transported from peripheral tissues and proliferated in the whole body of mice at this period.

3.3. Infection site of EV71 in small intestine

We dissected small intestines of mice into duodenum, jejunum and

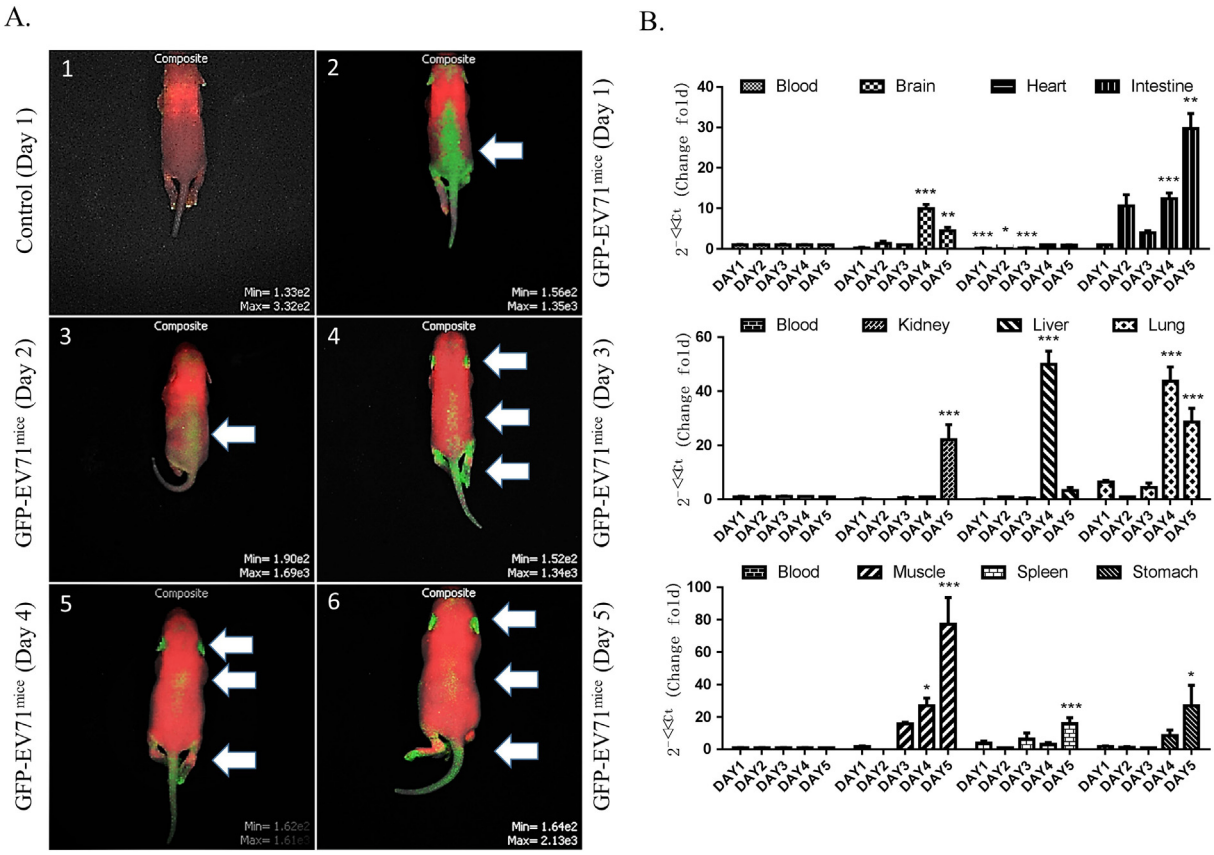

Fig. 2. Dynamic process assay of EV71 proliferating and transport in the whole body after oral-administration. (A) Daily detection of GFP fluorescence in suckling mice after oral-administrated with the adapted GFP-EV71 (MOI = 3). The result was displayed by LuminaIILiving Image System. (B) Measurement of virus titers of different tissues from oral-administrated suckling mice. The total RNA were extracted from different tissues every 24 h after oral-administration. The mRNA levels of EV71 were analyzed according to VP1 RNA sequence. The EV71 mRNA levels in blood were used as the negative control. *P* values were calculated by comparing other tissues with blood. $*P < .05$; $**P < .01$; $***P < .001$.

ileum to find out which part was the most susceptible to EV71 infection. qPCR and IHC techniques were used to detect EV71 proliferation in these three parts. According to Fig. 3A–C, mice ileum tissue was the most susceptible part to EV71. EV71 mRNA presented a consistently high level in ileum tissues in the following three days after oral-administration. The IHC experiments of ileum tissues showed strongest intensity of brown reactions against EV71-VP1 antibody. As shown in Fig. 3D–F, a high level of SCARB2 expression in ileum tissues was consistent with the presence of VP1 protein in ileum tissues. The ileum is the final section of small intestine, conducting major absorption function. The ileum owns the highest density of SCARB2, which resulted in the highest infection rate of EV71 in ileum tissues. However, ileum tissue alone could not indicate the process of EV71 transport and proliferation, due to the immediate and continuous infection, while jejunum displayed a relative slower infection process. As shown in Fig. 3A, EV71 mRNA levels increased gradually and reach the peak at the 60th hour, then decreased at the 72nd hour in jejunum tissues. Moreover, jejunum tissues only displayed brown reactions specific against EV71-VP1 antibody on the second and third days as shown in Fig. 3B. Differently, duodenum tissues showed observable brown reaction only on the third day, but ileum tissues presented obvious brown reaction from day one to day three. Therefore, jejunum tissue was used in further experiments analyzing the dynamic process of EV71.

3.4. Dynamic process of EV71 proliferation and transportation from small intestine

We speculated that the small intestine played a portal role, meaning its structural feature provided a gate to EV71 infection. To verify this hypothesis, we explored the dynamic process of EV71 proliferation from small intestine with the help of laser confocal microscope and IHC experiment. As mentioned before, jejunum tissue was suitable to conduct following experiments because we could trace the whole process of EV71 proliferation in jejunum tissues. Paraffin sections of jejunum tissue were made every 24 h after oral-administration. As shown in Fig. 4A and C, the intensity changes of GFP fluorescence indicated the whole process of EV71 entering bodies from intestines. The first day was the initial infection stage. Green fluorescence was shallow on section, which manifested small amount of EV71 infection in jejunum tissues. Plenty of GFP-EV71 virions might be excreted out of bodies at this time. The second day was the proliferation stage, for the increasing green fluorescence provided the evidence of rapid proliferation. The third day was the transport stage, due to the decay of green fluorescence. The fourth and fifth days were the proliferation-breakout stage, according to the afresh increasing green fluorescence. The brown reaction against EV71 VP1 antibody presented the same tendency as shown in Fig. 4B and D. The intensity of brown reaction increased sharply at the second day, decreased at the third day, and then recurred at the fourth and fifth days. These results were also consistent with Fig. 2's.

Furthermore, we observed that small intestinal villus was the main proliferation position from the slices. There was the higher intensity of green fluorescence and brown reaction in villus tissues than in intestinal walls as shown in Fig. 4. Obviously, the dense blood capillaries in small intestinal villi supply abundant nutrition and transport facility for EV71 proliferation and transport from small intestines. The epithelial cells widely distributing in small intestinal villi could be the infection gateway for EV71 entering host bodies.

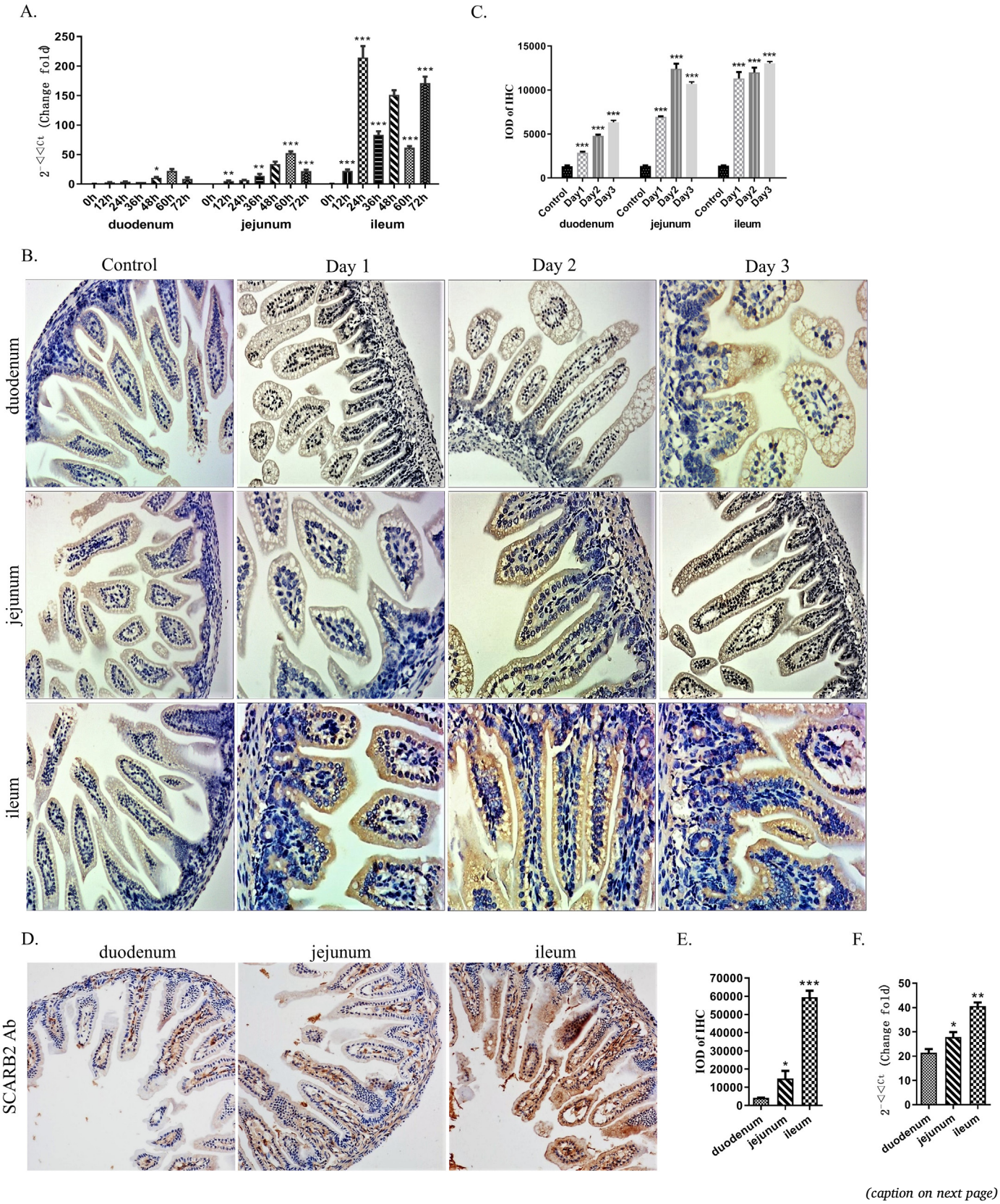

(caption on next page)

3.5. Physiological mechanism of EV71 infection in small intestine cells

We used three intestinal cell lines, CCD18-CO, DLD-1 and FHC respectively representing intestinal fibroblast, gland cell and epithelial cell, to explore the molecular mechanism of intestinal infection. In view of SCARB2 being the important receptor of EV71 (Yamayoshi et al., 2009), we analyzed the expression levels of SCARB2 protein in these intestinal cell lines and compared with several other tissue cell lines. As shown in Fig. 5A and B, the expression levels of SCARB2 protein were higher in these three intestinal cell lines, which provided more suitable

Fig. 3. Detection of small intestine infection sites after oral administration of EV71. (A) Measurement of virus titers in duodenum, jejunum and ileum tissues from oral-administrated suckling mice. The total RNA was extracted every 24 h after oral-administration. The mRNA levels of EV71 were analyzed according to VP1 RNA sequence. The EV71 mRNA levels at 0 h were used as negative control. *P* values were calculated by comparing other time with 0 h. *P < .05; **P < .01; ***P < .001. (A) Measurement of the expression of VP1 protein in duodenum, jejunum and ileum tissues by IHC staining. The intestinal tissues were sampled for IHC staining every 24 h after oral-administration. Anti-EV71-VP1 (GeneTex Ltd. Cat No. GTX132339) was used in IHC staining. (C) The expression quantifications of VP1 proteins were analyzed by Image-Pro Plus 6.0. IOD (Integrated Option Density) was estimated by calculating the area and the density of the brown color of IHC staining in Fig. 3B. *P* values were calculated by comparing other tissues with control tissues. *$P < .05$; **$P < .01$; ***$P < .001$. (D) Detection of the expressions of SCARB2 protein in duodenum, jejunum and ileum tissues by IHC staining. The intestinal tissues from untreated suckling mice were sampled for IHC staining. Anti-SCARB2 (Proteintech Ltd., Cat NO. 27102–1-AP) was used for IHC staining. (E) The expression quantifications of SCARB2 proteins were analyzed by Image-Pro Plus 6.0. IOD was estimated from the brown color in Fig. 3D. *P* values were calculated by comparing other tissues with duodenum tissues. *$P < .05$; ***$P < .001$. (F) Detection of the mRNA levels of SCARB2 in duodenum, jejunum and ileum tissues from untreated suckling mice. Analyses of triplicate experiments on each treatment were performed. *P* values were calculated by comparing other tissues with duodenum tissues. *P < .05; **$P < .01$. (For interpretation of the references to color in this figure legend, the reader is referred to the web version of this article.)

infection sites for EV71 in the intestine. However, the expression level of SCARB2 was not the main factor for EV71 infection in the intestine. Comparing with RD cells, these three intestinal cells exhibited relatively lower infection rates as shown in Fig. 5F (5G/5H/5I), indicating that the myofibroblasts like RD cell might be more susceptible to EV1 infection. We assumed that the intestine just played a portal role but not the main proliferation site.

Compared with CCD18-CO cells, DLD-1 and FHC cells displayed relatively higher infection rates as shown in Fig. 5F (5G/5H/5I), which indicated that EV71 entered intestinal villi through the fast infection of intestinal epithelial cells. To explore the significance of SCARB2 in EV71 infection, we knocked down SCARB2 from these three cells as shown in Fig. 5B and C. As the immunoblotting results of VP1 proteins shown, the knock-down cells with a low level of SCARB2 mRNA, displayed great resistance against EV71 infection effectively. The decreased levels of VP1 proteins suggested that SCARB2 protein was still the determinant factor of EV71 infection.

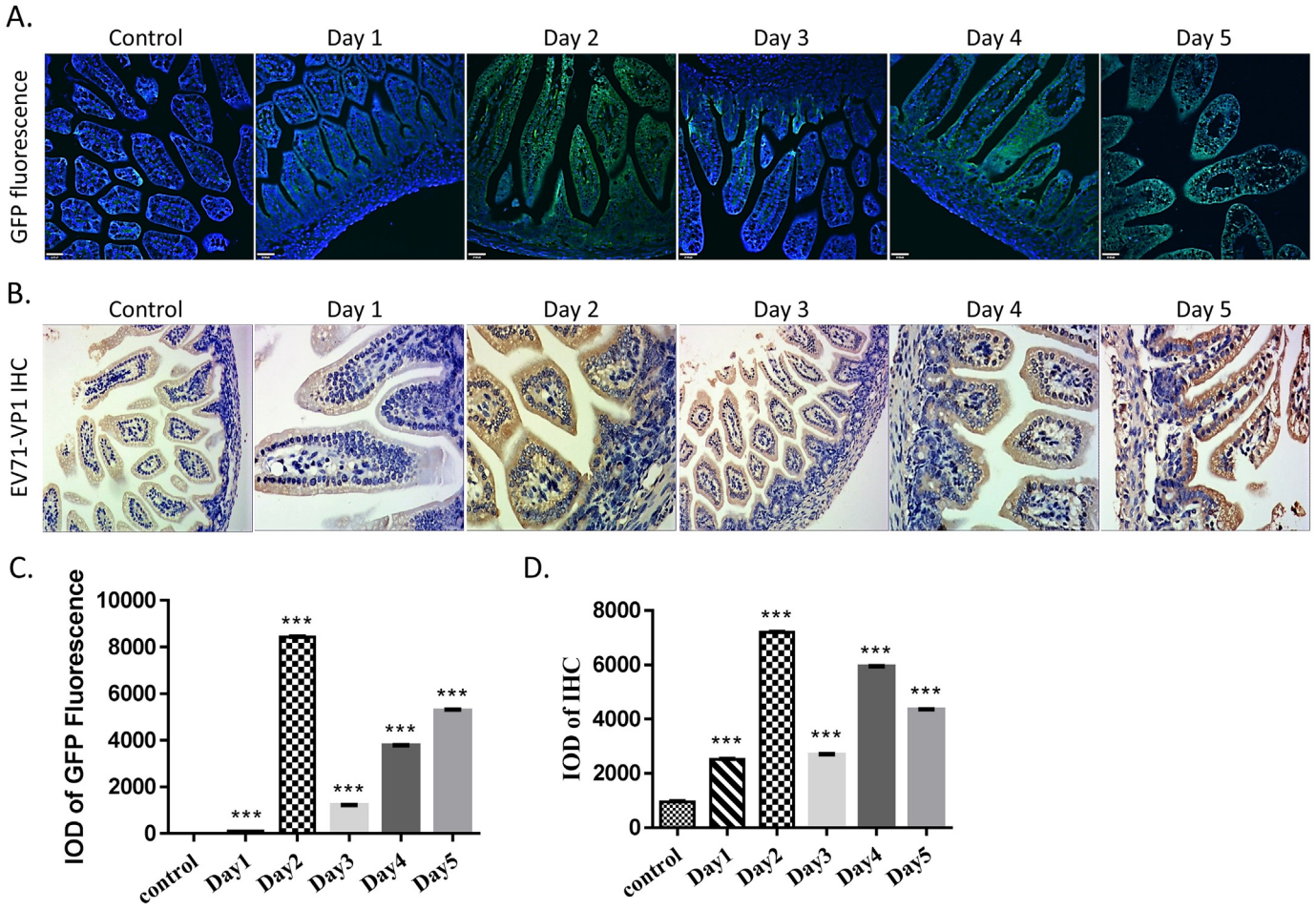

Fig. 4. Dynamic process assay of EV71 proliferating and transporting in small intestine after oral-administration. (A) Detection of GFP fluorescence in jejunum tissues every 24 h by micro examination of jejunum slices sampling. The mice were respectively oral-treated with 10 μl GFP-EV71 (MOI = 3). (B) Measurment of VP1 protein expression of jejunum tissues every 24 h by IHC staining. Anti-EV71-VP1 (GeneTex Ltd. Cat No. GTX132339) was used for IHC staining. (C) The expression quantifications of VP1 proteins were analyzed by Image-Pro Plus 6.0. IOD was estimated from the green fluorescence in Fig. 4A. P values were calculated by comparing other time point with control. ***$P < .001$. (D) The expression quantifications of VP1 proteins were analyzed by Image-Pro Plus 6.0. IOD was estimated from the brown color in Fig. 4B. P values were calculated by comparing other time point with control.***$P < .001$. (For interpretation of the references to color in this figure legend, the reader is referred to the web version of this article.)

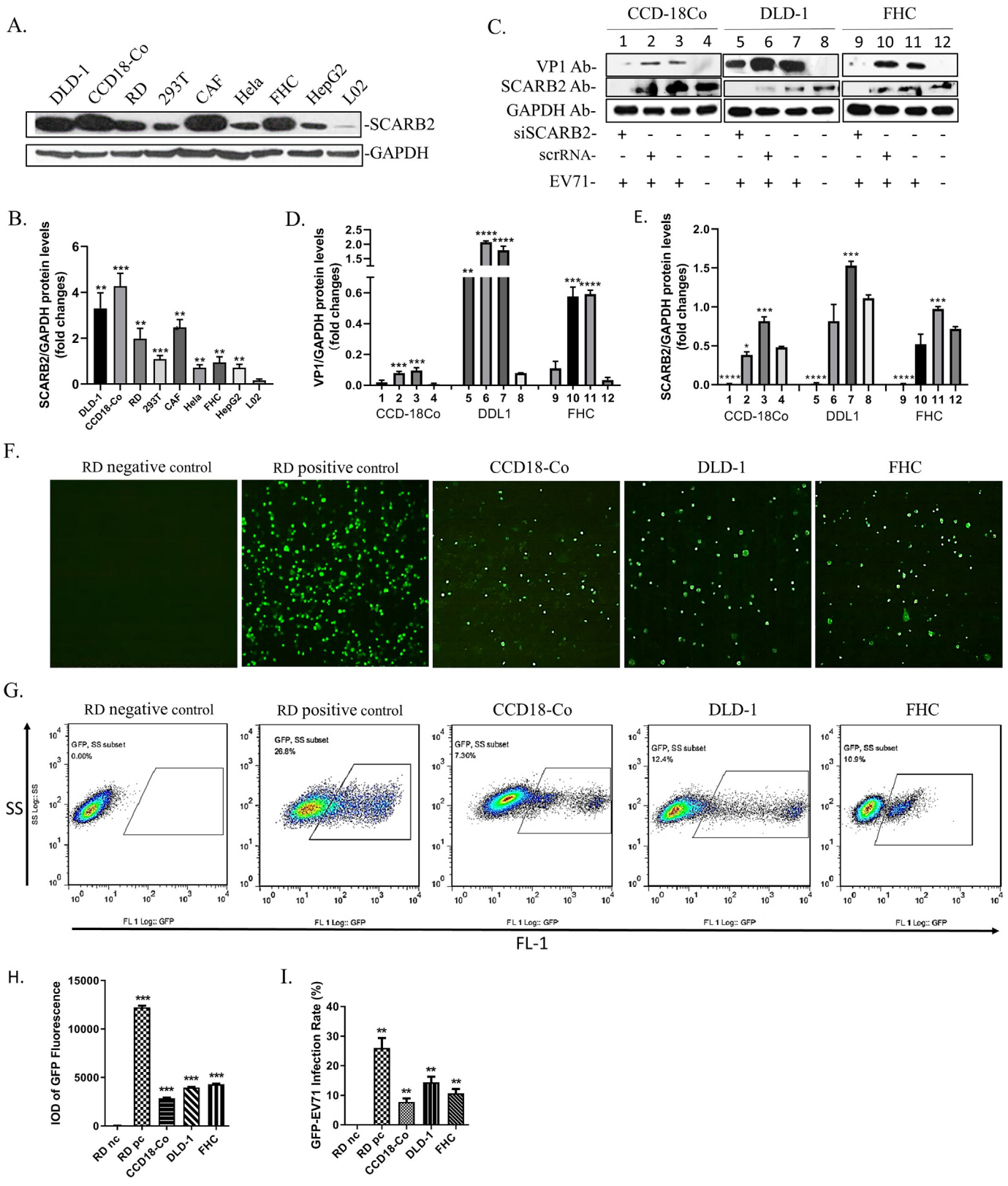

(caption on next page)

3.6. Preventive effect of acarbose against EV71 intestinal infection

A total of 72, one-day-old ICR mice were divided randomly into the negative control group (oral-administrated with normal saline), the positive control group (oral-administrated with EV71), the enhancer group (oral-administrated with both sodium caprate and EV71) and the inhibitor group (oral-administrated with both acarbose and EV71). 18 mice were distributed in each group. EV71 mRNA was detected by qPCR technology to measure the change of EV71 titer in different intestinal parts every 12 h.

Fig. 5. Cellular physiological mechanism of EV71 infection in small intestine. (A) Western Blot experiment and (B) the relative quantification for SCARB2 protein expression in various cell lines. P values were calculated by comparing various cell lines with L02 cell line. $^{**}P < .01$; $^{***}P < .001$. (C) Western Blot experiment and (D, E) the relative quantification for protein expression of EV71 VP1 and SCARB2 in CCD-18Co, DLD-1 and FHC cell lines. SCARB2 proteins were knocked down by siSCARB2. After 24 h, cells were infected by EV71 (MOI = 3), and then cultured for 36 h. P values were calculated by comparing infected cells with non-infected cells in the respective cell lines. $^{**}P < .01$; $^{***}P < .001$; $^{****}P < .0001$. (F) Verifying EV71 infection efficiency of the intestinal cells through microscopic examination of GFP fluorescence in intestinal cells. The subject cells had been infected by GFP-EV71 (MOI = 3) for 36 h. RD cell line was use as the control. (G) Verifying EV71 infection efficiency of the intestinal cells through counting the number of fluorescent cells by flow cytometry. The subject cells had been infected by GFP-EV71 (MOI = 3) for 36 h. RD cell line was use as the control. (H) The quantifications of GFP fluorescence were analyzed by Image-Pro Plus 6.0. IOD was estimated from the green fluorescence in Fig. 5F. Analyses of triplicate experiments on each treatment were performed. P values were calculated by comparing various cell lines with non-infected RD cells. $^{***}P < .001$. (I) GFP-EV71 infection rates were analyzed according to Fig. 5G. Analyses of triplicate experiments on each treatment were performed. P values were calculated by comparing various cell lines with non-infected RD cells. $^{**}P < .01$. (For interpretation of the references to color in this figure legend, the reader is referred to the web version of this article.)

As shown in Fig. 6A, acarbose significantly pulled down the titer of EV71 in all three parts of the small intestine, while sodium caprate accelerated EV71 infection by contrast. Compared with the positive control group, duodenum tissue in the inhibitor group did not present any accumulation of EV71 until 60-h of infection, but the enhancer group displayed obvious increase of EV71 mRNA after 12-h of infection period. Three groups achieved the peak level of EV71 mRNA at the same time, which was the 60th hour as shown in figure 6A1. At that time, the EV71 mRNA ratio of the inhibitor, positive control and enhancer groups was 0.8: 1.0: 1.53. As shown in figure 6A2, three groups presented the similar proliferation tendency in jejunum tissue, but the enhancer group reached the mRNA peak at the 36th hour, which was 12 h earlier than the other two groups. EV71 mRNA maintained relatively higher level in ileum tissue than in other two intestinal parts during the whole infection process as shown in figure 6A3. The inhibitor group still presented relatively lower level of EV71 mRNA than other two groups in ileum tissue.

The preventive effect of acarbose was further tested at the cellular level. The three intestinal cell lines were respectively treated by acarbose (1.5 μg/ml) and sodium caprate (1.5 μg/ml), and then were infected with GFP-EV71 (MOI = 3). Cells infected with GFP-EV71 alone were used as the positive control. Cells without any treatment were used as the negative control. As shown in Fig. 6B and C, according to the immunoblotting results, the expression level of VP1 protein was lower in the acarbose-treated CCD18-Co cells than in the positive control, while the sodium-caprate-treated CCD18-Co cells displayed a higher expression level of VP1 protein by contrast. DLD-1 and FHC cells showed the same expression trend of VP1 protein as CCD18-Co cells. The knock-down of SCARB2 protein also decreased the infection of EV71 in DLD-1 and FHC cells.

In order to further prove the opposite effect of acarbose and sodium caprate on EV71 infection, we knocked down SCARB2 proteins of DLD-1, FHC and CCD18-Co cells. To conduct the knock-down process, cells cultured in a 60-mm culture vessel were transfected with 50 nmol of siSCARB2 by using Lipofectamine 2000 (ThermoFisher Ltc. Cat No. 11668019). After 48 h' incubation, cells were subsequently infected with EV71 (MOI = 3), and treated with acarbose (1.5 μg/ml) or sodium caprate (1.5 μg/ml) during the next 24 h. According to the immunoblotting results shown in Fig. 6D (6E and 6F), SCARB2-knocked-down CCD18-Co cells displayed lower VP1 protein levels than other CCD18-Co cells. Among the SCARB2-knocked-down CCD18-Co cells, VP1 protein bands were fainter in acarbose-treated cells than in only EV71-infected cells. Interestingly, after the knock-down of SCARB2, the band of VP1 protein were relatively stronger in sodium-caprate-treated cells than in only EV71-infected cells. DLD-1 and FHC cells even displayed same trend as shown in Fig. 6D (6E and 6F). Obviously, SCARB2 protein is not the only factor for intestinal infection of this adapted EV71. Sodium caprate still promoted the increase of infection rates even if SCARB2 genes were knocked down in these three intestinal cell lines, which suggested that EV71 could infect cells through other mechanisms. We inferred that the mutations of specific amino acids in the capsid proteins of the adapted EV71 increase the chance of glycosylation of the virus so that EV71 can infect cells through binding with cell surface receptors of saccharide groups. On the other sides, the abundant villi of the small intestine will facilitate the encapsulation of the virus. Some viruses may have entered small intestinal cells directly through endocytosis.

4. Discussion

HFMD is usually caused by CVA16 and EV71 (Aswathyraj et al., 2016). Early symptoms of HFMD may include fever and a sore throat. Painful blisters can usually show up in the back portion of the mouth or tongue (Khan et al., 2019). Obviously, the nose and mouth are the main entries of infection for EV71 virus to invade human body. Rash will appear on the palms of children's hands or the soles of their feet a day or two after the first symptoms appear(Khan et al., 2019). Based on mouse model of EV71 infection, we achieved the results consistent with clinical symptoms. As shown in Fig. 2A and B, EV71 firstly transported into intestinal tissues of mice at the second day after oral-administration. Then EV71 quickly transported into peripheral tissues at the third day. Thus, peripheral tissue is the second stage of EV71 infection *in vivo*.

According to the clinical studies, EV71 can cause more severe neurological complications compared with other enterovirus serotypes, including brainstem encephalitis and acute flaccid paralysis (Hu et al., 2015). Severe infection of EV71 even can cause pneumonia, hepatosplenomegaly, liver calcification, excessive ascites, and mild hydrocephalus (Chow et al., 2000; Li and Lao, 2017; Ooi et al., 2010). Our results also support these clinical symptoms. As shown in Fig. 2A and B, the fourth and fifth days were the outbreak period in the whole bodies of mice. EV71 already transported and proliferated in the whole bodies of mice at this period. EV71 mRNA has been detected in many important mice tissues including brain, intestine, kidney, liver, lung, muscle, spleen and stomach.

Yi-Chun Chen and Huan-Yao Lei et al. also proved the dynamic transfer pathway of EV71 through a murine oral EV71 infection model (Chen et al., 2004). They revealed that EV71 replicated first in the small intestine, and then induced viraemia and spread to various organs. Their kinetic studies showed that EV71 antigen was first detected in the intestine at 6 h, in the thoracic spinal cord at 24 h, in the cervical spinal cord at 50 h and in the brain stem at 78 h post-infection. Their results also indicated that intestinal infection is the gateway for EV71 to invade the whole body. We also verified that ileum was the primary site of infection and transfer in small intestine of mice as shown in Fig. 3A–C. Ileum tissues displayed more SCARB2 protein expression in the results of immunohistochemistry (IHC) experiment as shown in Fig. 3D–F. As the cellular receptor of EV71, more SCARB2 expression means more rapid intestinal infection of EV71. EV71 will metastase rapidly after the infection of small intestine as shown in Fig. 4. EV71 entered the villous tissue of small intestine through the infection of intestinal epithelial cell as displayed in Fig. 5. Then EV71 quickly entered blood vessels and spread to various organs, which was also confirmed by Lintao Cai et al. (Pan et al., 2018). Therefore, the suppression of intestinal infection will effectively prevent the infection of EV71 to the whole body.

As Zihe Rao's reports (Dang et al., 2014), EV71 infect the host cells by interacting with the canyon region of its virion surface and the

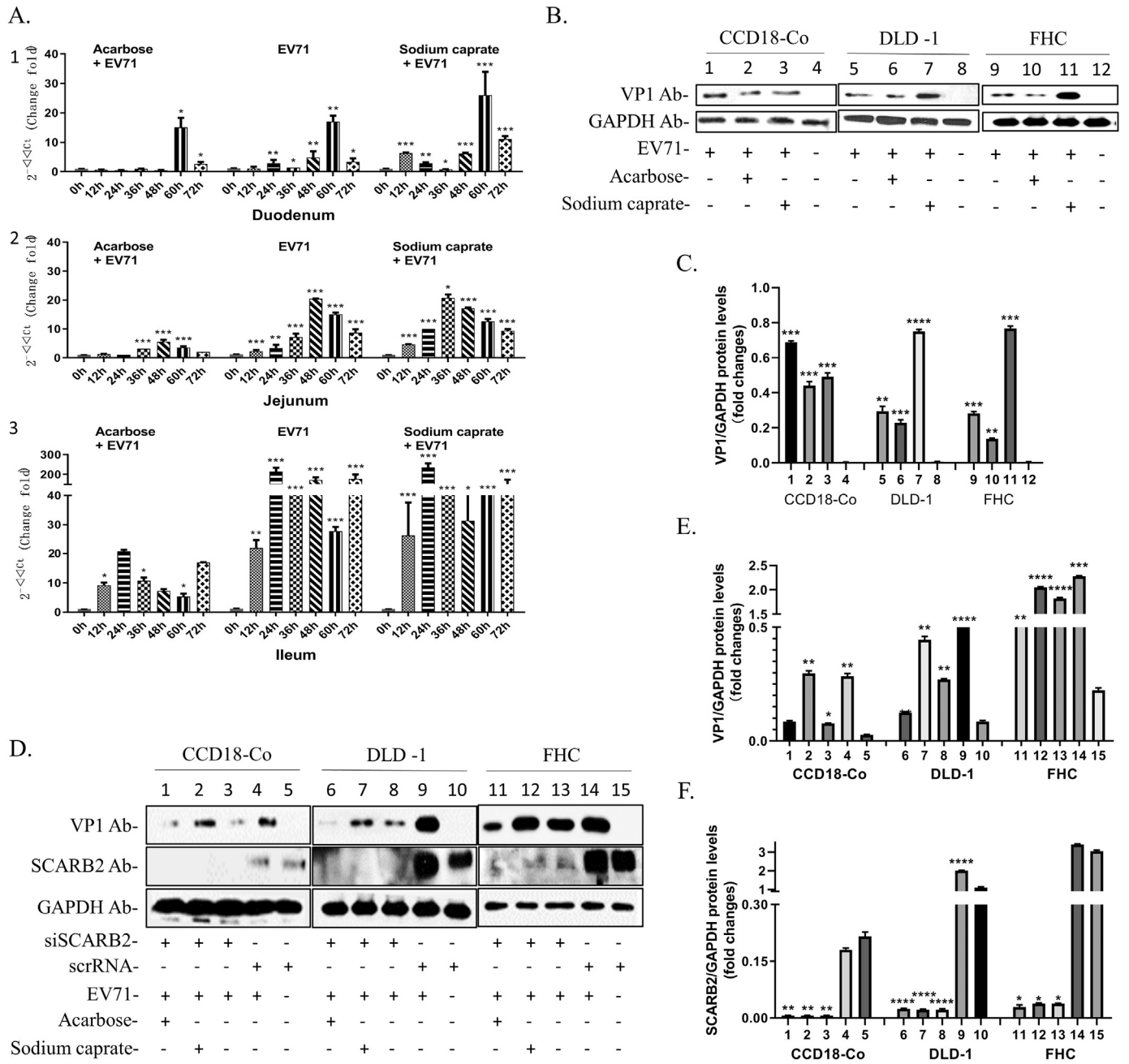

Fig. 6. Explore prevention possibility of intestinal infection by acarbose. Sodium caprate was used as the positive control. (A) Verifying the blocking efficiency of acarbose on EV71 infection in duodenum, jejunum and ileum tissues. The total RNA was respectively extracted every 12 h after oral-administration. The mRNA levels of VP1 were analyzed according to VP1 RNA sequence. The EV71 mRNA levels at 0 h were used as the negative control. Analyses of triplicate experiments on each treatment were performed. *P* values were calculated by comparing other time point with 0 h. **P* < .05; ***P* < .01; ****P* < .001. (B) Verifying the blocking effects of acarbose on CCD-18Co, DLD-1 and FHC cell lines through measuring the expression levels of VP1 protein by Western Blot experiment. Cells were firstly treated respectively by acarbose and sodium caprate for 12 h, and then were infected by GFP-EV71 for 36 h. (C) the relative quantification for EV71 VP1 protein expression in CCD18-Co, DLD-1 and FHC cell lines. Grey scales of protein bands from Fig. 6B were detected by ImageJ 6. P values were calculated by comparing infected cells with non-infected cells in the respective cell lines. **P < .01; ***P < .001. (D) Verifying the blocking effects of acarbose and siSCARB2 on CCD-18Co, DLD-1 and FHC cell lines through measuring the expression levels of VP1 protein by immunoblotting. Cells were firstly transfected by siSCARB2 for 24 h, then respectively treated by acarbose and sodium caprate for 12 h, and then infected by GFP-EV71 for 36 h. (E) and (F) the relative quantification for protein expression of EV71 VP1 and SCARB2 in CCD18-Co, DLD-1 and FHC cell lines. Grey scales of protein bands from Fig. 6D were detected by ImageJ 6. P values were calculated by comparing infected cells with non-infected cells in the respective cell lines. *P < .05; **P < .01; ***P < .001; ****P < .0001.

modified glycosyl of cellular SCARB2 protein. So the suitable sugar molecules will be the potential competitive inhibitors to block glycosyl-binding sites on the virion surface of EV71. Acarbose, as a glucose channel inhibitor, can efficiently block glucose absorption in intestines. With more pyran glucose groups, acarbose has the potential to inhibit the recruitment of the glycosyl of SCARB2 proteins. The mutations of capsid proteins of the adapted EV71 increase the glycosylation rate of EV71 surface, which suggests that EV71 can infect host cells through binding with cell surface receptors of saccharide groups. Acarbose inhibits exactly these receptors to prevent EV71 infection. Acarbose also displayed inhibitory effect on maltose absorption in rat intestine (Luo et al., 2001), and has been applied in clinic, presenting low toxic and

few side effects. So we chose acarbose as the cure for EV71 intestine infection. Meanwhile, sodium caprate is a common intestinal absorption enhancer(Lv et al., 2010), which was used as the positive control. As shown in Fig. 6, acarbose effectively decreased the titer of EV71 in three parts of small intestine. Sodium caprate, on the contrary, accelerated EV71 infection in the whole small intestine. Therefore, we confirmed that acarbose or its analogue will be the potential medicines to prevent EV71 infection.

5. Conclusion

Though the conditions of human body are more complicated than mouse model, we can still obtain some inspiration from our results. EV71 infection pathways are diverse and unpredictable, besides cleaning and disinfection, no effective cure has been found. Since the main pathway of EV71 infection is through oral cavity, it is very important to figure out the dynamic physiological process of EV71 transport from mouth to the whole body. We have explored its physiological pathway, transport direction, proliferation lifecycle, key nods and primary proliferation tissues in the infection process. To conclude, the small intestine is the gateway for EV71 infection. Small intestinal villi are the main positions for EV71 to proliferate and transport *in vivo* at the early infection stage. Peripheral muscle tissues were the second transport station. Then, overall infection broke out in the whole body after EV71 proliferated in peripheral muscle tissues. Therefore, it will be a creative way to prevent EV71 intestine infection. Though acarbose can effectively inhibit EV71 intestine infection as verified before, the generalisability of these results is subject to certain limitations. For instance, more work need to be done to verify the molecular mechanism of acarbose inhibiting EV71. Moreover, follow-up work including treatment method, clinical trial and new allied drug development need to be done further. These following studies will help to develop new blocking agents and new therapy method.

Funding

This work was supported by Grants from National Natural Science Foundation of China (Nos. 30800190, 81372441), and State Key Laboratory of Virology of China.

Availability of data and materials

The datasets analyzed in this study are available from the corresponding author upon reasonable request.

Ethics approval and consent to participate

The report data in this manuscript were collected from suckling mice. The Ethics Committee of Wuhan University (ECWU) in China authorized all of the experiments in the manuscript. We consent to participate under the 'Ethics, consent and permissions' heading.

CRediT author statement

Qingyuan Feng, Huiting Zhou, Jie Wang and Cuiping Zhang conceived and designed the experiments, performed the experiments.

Huiting Zhou and Xuan Liu analyzed the data, and wrote the paper.

Xiaojing Ma and Chunju Quan performed virus culture and purification.

Xiyue Zhang performed the mutation.

Xiyue Zhang and Qingyuan Feng carried out supplementary experiments.

Zhongliang Zheng and Xiyue Zhang revised and approved the final manuscript.

Declaration of Competing Interest

The authors declare that they have no competing interests.

Acknowledgments

We thank Yi Dong, PhD for assistance with confocal microscopy analyses, and Ying-ge Li for assistance with immunohistochemistry assays.

References

Aswathyraj, S., Arunkumar, G., Alidjinou, E.K., Hober, D., 2016. Hand, foot and mouth disease (HFMD): emerging epidemiology and the need for a vaccine strategy. Med. Microbiol. Immunol. 205, 397–407.

Caine, E.A., Moncla, L.H., Ronderos, M.D., Friedrich, T.C., Osorio, J.E., 2016. A single mutation in the VP1 of Enterovirus 71 is responsible for increased virulence and Neurotropism in adult interferon-deficient mice. J. Virol. 90, 8592–8604.

Chang, H.W., Lin, Y.W., Ho, H.M., Lin, M.H., Liu, C.C., Shao, H.Y., Chong, P., Sia, C., Chow, Y.H., 2013. Protective efficacy of VP1-specific neutralizing antibody associated with a reduction of viral load and pro-inflammatory cytokines in human SCARB2-transgenic mice. PLoS One 8, e69858.

Chen, Y.C., Yu, C.K., Wang, Y.F., Liu, C.C., Su, I.J., Lei, H.Y., 2004. A murine oral enterovirus 71 infection model with central nervous system involvement. J. Gen. Virol. 85, 69–77.

Chen, C.S., Yao, Y.C., Lin, S.C., Lee, Y.P., Wang, Y.F., Wang, J.R., Liu, C.C., Lei, H.Y., Yu, C.K., 2007. Retrograde axonal transport: a major transmission route of enterovirus 71 in mice. J. Virol. 81, 8996–9003.

Chow, K.C., Lee, C.C., Lin, T.Y., Shen, W.C., Wang, J.H., Peng, C.T., Lee, C.C., 2000. Congenital Enterovirus 71 infection: a case study with virology and immunohistochemistry. Clin. Infect. Dis. 31, 509–512.

Cong, H., Du, N., Yang, Y., Song, L., Zhang, W., Tien, P., 2016. Enterovirus 71 2B induces cell apoptosis by directly inducing the conformational activation of the Proapoptotic protein Bax. J. Virol. 90, 9862–9877.

Dang, M., Wang, X., Wang, Q., Wang, Y., Lin, J., Sun, Y., Li, X., Zhang, L., Lou, Z., Wang, J., Rao, Z., 2014. Molecular mechanism of SCARB2-mediated attachment and uncoating of EV71. Protein Cell 5, 692–703.

Gao, F., Wang, Y.P., Mao, Q.Y., Yao, X., Liu, S., Li, F.X., Zhu, F.C., Yang, J.Y., Liang, Z.L., Lu, F.M., Wang, J.Z., 2012. Enterovirus 71 viral capsid protein linear epitopes: identification and characterization. Virol. J. 9, 1–7.

He, S.J., Han, J.F., Ding, X.X., Wang, Y.D., Qin, C.F., 2013. Characterization of enterovirus 71 and coxsackievirus A16 isolated in hand, foot, and mouth disease patients in Guangdong, 2010. Int. J. Infect. Dis. 17.

Hu, Y., Jiang, L., Peng, H.L., 2015. Clinical analysis of 134 children with nervous system damage caused by Enterovirus 71 infection. Pediatr. Infect. Dis. J. 34, 718–723.

Hung, H.C., Shih, S.R., Chang1, T.-Y., Fang, M.-Y., Hsu, J.T.-A., 2014. The combination effects of licl and the active leflunomide metabolite, A771726, on viral-induced interleukin 6 production and EV-A71 replication. PLoS One 9, e111331.

Khan, M.A.H., Anwar, K.S., Muraduzzaman, A.K.M., Mollah, M.A.H., Akhter-ul-Alam, S.M., Islam, K.M., Hoque, S.A., Islam, M.N., Ali, M.A., 2019. Emerging hand foot mouth disease in bangladeshi children- first report of rapid appraisal on pocket outbreak: clinico-epidemiological perspective implicating public health emergency. F1000Research 7, 1–25.

Khong, W.X., Yan, B., Yeo, H., Tan, E.L., Lee, J.J., Ng, J.K.W., Chow, V.T., Alonso, S., 2012. A non-mouse-adapted enterovirus 71 (EV71) strain exhibits neurotropism, causing neurological manifestations in a novel mouse model of EV71 infection. J. Virol. 86, 2121–2131.

Kim, C., Kang, H., Kim1, D., Song, J.-H., Choi, M., Kang, M., Lee, K., Kim, H.S., Shin, J.S., Jeong, H., Jung, S., Han, S.-B., Kim, J.H., Ko, H.-J., Lee, C.-K., Kim, M., Cho, S., 2016. Antiviral activity of micafungin against enterovirus 71. Virol. J. 13, 99.

Kobayashi, K., Sudaka, Y., Takashino, A., Imura, A., Fujii, K., Koike, S., 2018. Amino acid variation at VP1-145 of enterovirus 71 determines attachment receptor usage and neurovirulence in human scavenger receptor B2 transgenic mice. J. Virol. 92 (15) pii. e00681-18.

Lee, K.Y., 2016. Enterovirus 71 infection and neurological complications. Korean J Pediatr 59, 395–401.

Lei, X., Xiao, X., Zhang, Z., Ma, Y., Qi, J., Wu, C., Xiao, Y., Zhou, Z., He, B., Wang, J., 2017. The Golgi protein ACBD3 facilitates Enterovirus 71 replication by interacting with 3A. Sci. Rep. 7, 44592.

Li, H.-G., Lao, Q., 2017. The pulmonary complications associated with EV71-infected handefootemouth disease. Radiology of Infectious Diseases 4, 137–142.

Li, X., Fan, P., Jin, J., Su, W., An, D., Xu, L., Sun, S., Zhang, Y., Meng, X., Gao, F., Kong, W., Jiang, C., 2013. Establishment of cell lines with increased susceptibility to EV71/CA16 by stable overexpression of SCARB2. Virol. J. 10, 1–11.

Li, B., Yue, Y., Zhang, Y., Yuan, Z., Li, P., Song, N., Lin, W., Liu, Y., Gu, L., Meng, H., 2017. A novel Enterovirus 71 (EV71) virulence determinant: the 69th residue of 3C protease modulates pathogenicity. Front. Cell. Infect. Microbiol. 7, 26.

Lin, Y.W., Yu, S.L., Shao, H.Y., Lin, H.Y., Liu, C.C., Hsiao, K.N., Chitra, E., Tsou, Y.L., Chang, H.W., Sia, C., Chong, P., Chow, Y.H., 2013. Human SCARB2 transgenic mice as an infectious animal model for enterovirus 71. PLoS One 8, e57591.

Lin, P., Gao, L., Huang, Y., Chen, Q., Shen, H., 2015. An enterovirus 71 strain causes skeletal muscle damage in infected mice. Int. J. Clin. Exp. Pathol. 8, 3460–3468.

Luo, H., Wang, L.F., Imoto, T., Hiji, Y., 2001. Inhibitory effect and mechanism of acarbose combined with gymnemic acid on maltose absorption in rat intestine. World J. Gastroenterol. 7, 9–15.
Lv, X., Li, J., Zhang, M., Wang, C., Fan, Z., Wang, C., Chen, L., 2010. Enhancement of sodium Caprate on intestine absorption and antidiabetic action of Berberine. AAPS PharmSciTech 11, 372–382.
Lyu, K., Wang, G.C., He, Y., Han, J.F., Ye, Q., Qin, C.F., Chen, R., 2015. Crystal structures of enterovirus 71 (EV71) recombinant virus particles provide insights into vaccine design. J Biol Chem. 290 (6), 3198–3208.
Ooi, M.H., Wong, S.C., Lewthwaite, P., Cardosa, M.J., Solomon, T., 2010. Clinical features, diagnosis, and management of enterovirus 71. Lancet Neurol. 9, 1097–1105.
Pan, H., Yao, X., Chen, W., Wang, F., He, H., Liu, L., He, Y., Chen, J., Jiang, P., Zhang, R., Ma, Y., Cai, L., 2018. Dissecting complicated viral spreading of enterovirus 71 using in situ bioorthogonal fluorescent labeling. Biomaterials 181, 199–209.
Solomon, T., Lewthwaite, P., Perera, D., Cardosa, M.J., McMinn, P., Ooi, M.H., 2010. Virology, epidemiology, pathogenesis, and control of enterovirus 71. Lancet Infect. Dis. 10, 778–790.
Song, J., Hu, Y., Li, J., Zheng, H., Wang, J., Guo, L., Shi, H., Liu, L., 2018. Suppression of the toll-like receptor 7-dependent type I interferon production pathway by autophagy resulting from enterovirus 71 and coxsackievirus A16 infections facilitates their replication. Arch. Virol. 163, 135–144.
Victorio, C.B.L., Yishi Xu1, Q.N., Meng, T., Chow, V.T., Chua, K.B., 2016. Cooperative effect of the VP1 amino acids 98E, 145A and 169F in the productive infection of mouse cell lines by enterovirus 71 (BS strain). Emerg Microbes Infect e60, 5.
Xu, F., Zhao, X., Hu, S., Li, J., Yin, L., Mei, S., Liu, T., Wang, Y., Ren, L., Cen, S., Zhao, Z., Wang, J., Jin, Q., Liang, C., Ai, B., Guo, F., 2016. Amphotericin B inhibits Enterovirus 71 replication by impeding viral entry. Sci. Rep. 6, 33150.
Yamayoshi, S., Yamashita, Y., Li, J., Hanagata, N., Minowa, T., Takemura, T., Koike, S., 2009. Scavenger receptor B2 is a cellular receptor for enterovirus 71. Nat. Med. 15, 798–801.
Yao, Xin, Mao, Q., Li, Y., Hao, C.S., Bian, L., Chen, P., Gao, F., Wu, X., Lu, W.W., Gao, Q., Li, X., Liang, Z.L., 2018. Poorly neutralizing polyclonal antibody in vitro against coxsackievirus A16 circulating strains can prevent a lethal challenge in vivo. Hum Vaccin Immunother 14, 1275–1282.
Yi, E.J., Shin, Y.J., Kim, J.H., Kim, T.G., Chang, S.Y., 2017. Enterovirus 71 infection and vaccines. Clin Exp Vaccine Res 6, 4–14.
Zeng, H., Wen, F., Huang, W., Gan, Y., Zeng, W., Chen, R., He, Y., Wang, Y., Liu, Z., Liang, C., Wong, K.K.L., 2016. New findings, classification and long-term follow-up study based on MRI characterization of brainstem encephalitis induced by Enterovirus 71. PLoS One 11, e0162877.
Zhang, X., Song, Z., Qin, B., Zhang, X., Chen, L., Hua, Y., Yuan, Z., 2013. Rupintrivir is a promising candidate for treating severe cases of enterovirus-71 infection: evaluation of antiviral efficacy in a murine infection model. Antivir. Res. 97, 264–269.
Zhao, F.R., Xie, Y.L., Liu, Z.Z., Shao, J.J., Li, S.F., Zhang, Y.G., Chang, H.Y., 2017. Lithium chloride inhibits early stages of foot-and-mouth disease virus (FMDV) replication in vitro. J. Med. Virol. 89, 2041–2046.
Zhou, F., Kong, F., Wang, B., McPhie, K., L, G., Gilbert Dwyer, D.E., 2011. Molecular characterization of enterovirus 71 and coxsackievirus A16 using the 5′ untranslated region and VP1 region. J Med Microbiol 60, 349–358.